PCCP

Cite this: *Phys. Chem. Chem. Phys.*, 2011, **13**, 7467–7474

www.rsc.org/pccp

PAPER

Capping polymer-enhanced electrocatalytic activity on Pt nanoparticles: a combined electrochemical and *in situ* IR spectroelectrochemical study†

Ceren Susut,[a] De-Jun Chen,[ab] Shi-Gang Sun*[b] and YuYe J. Tong*[a]

Received 19th January 2011, Accepted 1st March 2011
DOI: 10.1039/c1cp20164f

Unexpected yet highly remarkable and intriguing observations of the polymer-enhanced electro-catalytic activity of the Pt nanoparticles for electro-oxidations of both methanol and formic acid were reported. *In situ* FTIR investigation suggests strongly that the observed activity enhancements are highly likely due to the PVP-induced additional reaction pathways. These observations may open up a new paradigm of research in which the protecting/stabilizing organic ligands can now be incorporated as an advantageous part and/or a finer catalytic activity tuner of a nanocatalytic system.

1. Introduction

Exquisite control of shape and size of metal nanoparticles (NPs) is *essential* in achieving rational design of heterogeneous catalysts in general and electrocatalysts in particular. Polymers and organic ligands such as poly(vinylpyrrolidone) (PVP) are crucial in this regard in the colloidal synthesis of metal NPs and are particularly important in maintaining the post-synthesis stability of the shape and size of the metal NPs. In homogeneous catalysis, the catalytic properties of the polymer capped NPs are studied without the removal of the organic shell.[1,2] Moreover, tuning the solution-phase catalytic activity of these particles through the manipulation of the organic ligands is well-documented.[3] In contrast, in heterogeneous catalysis which includes fuel cell catalysis, the capping polymer is usually considered to hamper the catalytic activity therefore it is customary to remove it prior to catalysis,[4–6] usually at the expense of the well-defined shape and size. However, recent works showed that not only the metal NPs are catalytically active in the presence of the capping polymer but also certain capping polymers can enhance their catalytic activity for various fuel-cell reactions.[7–10]

An illustrative example is from our recent work in which we studied the CO and methanol (MeOH) electro-oxidation (EO) reactions on Pt NPs exposing two dominant crystallographic orientations, namely; (100) and (111).[9] The cubic and octahedral/tetrahedral shaped particles were synthesized *via* a modified polyol synthesis procedure that employed PVP as the surface capping agent.[11] As our efforts to find an efficient post-synthesis treatment to remove the PVP completely while avoiding the loss of the defined size and shape of the NPs turned out to be futile, we treated our particles by a method that eliminated the majority of the PVP. Thermal gravimetric analysis (TGA) revealed that the remaining PVP content was about 15% (wt) of the samples but the shape and size of the Pt NPs were well preserved.[9] Even under these circumstances, we observed that the Pt NPs enclosed dominantly with (111) nanofacets demonstrated an activity for the EO of MeOH about 4 times higher than that of commercial Pt black.[9]

While somewhat unexpected, these observations raise an interesting prospect of developing a practically important operando that may harness simultaneously the structural stabilizing and catalytic activity tuning capabilities of the capping polymer, which is the central theme of this paper. More specifically, we report the results of our combined electrochemical (EC) and *in situ* IR spectroelectrochemical investigation regarding the effect of the adsorbed PVP on the catalytic activity of a well-known industrial electrocatalyst for fuel cell applications—the Johnson-Matthey Pt black. The results showed clearly that the adsorbed PVP had the ability to enhance significantly the catalytic activity of the underlying Pt black towards *both* MeOH and formic acid (FA) EOs and the degree of the enhancement was tunable by varying the PVP content.

2. Experimental

Synthesis

For our study, two different samples were prepared; the starting material for each was commercially available Pt black (courtesy of Johnson-Matthey, average diameter 3 nm). For consistency, Pt black/PVP NP catalysts were prepared by following the polyol-based synthetic procedure that was employed to synthesize Pt NPs of different shapes.[9,11] The procedure was modified in such a way that commercially available Pt black

[a] *Department of Chemistry, Georgetown University, 37th & O Streets, NW, Washington DC, 20057, USA. E-mail: yyt@georgetown.edu*
[b] *State Key Laboratory of Physical Chemistry of Solid Surfaces, College of Chemistry and Chemical Engineering, Xiamen University, Xiamen 361005, China. E-mail: sgsun@xmu.edu.cn*
† Electronic supplementary information (ESI) available. See DOI: 10.1039/c1cp20164f

replaced H_2PtCl_6. EG (ethylene glycol) solutions of PVP and Pt black were added into the boiling EG in 2 different ratios (PVP/Pt: 12 and 24 molar ratios after which the samples were named as Pt–PVP12 and Pt–PVP24 respectively) and the mixture was refluxed for 1 h. After the reaction, the unreacted PVP was removed by repetitive centrifugation and precipitation. The PVP content in a given amount of catalyst sample was determined by TGA (TA Instruments Q 50). The sample and reference were placed in the furnace which was blanketed by a steady flow of nitrogen (20 ml min^{-1}). The experiments ensued at room temperature and climbed at a rate of 10 °C min^{-1} to a final temperature of 1000 °C. Analysis was performed *via* the Universal TA Analysis 2000 software. The TGA data (Fig. S1, curves a and b, respectively, in ESI†) revealed that 7.8 wt% of a given Pt–PVP12 sample was PVP whereas Pt–PVP24 contained 12.3 wt% of PVP.

EC measurements

For EC measurements, the catalyst dispersions were prepared by following the procedure described elsewhere[12] with a slight modification.[9] Briefly 2.5 mg of catalyst was ultrasonically dispersed in 0.5 ml of an aqueous solution containing 0.2 ml of iso-propanol and 0.002 ml of a 5 wt% Nafion solution. 20 μl of these inks were drop-cast onto a well-polished home-made glassy carbon (GC) electrode of 5 mm diameter and air-dried (loading amount was calculated as 0.1 mg for each sample). All EC experiments were carried out in an Ar-blanketed conventional three-electrode electrochemical cell using a CHI electrochemical workstation (CHI 660C). Unless otherwise noted, all CVs were recorded with a scan rate of 50 mV s^{-1}. A Pt wire and Ag/AgCl (3 M) were used as counter and reference electrodes, respectively. The supporting electrolytes used were 0.5 M or 0.1 M (for FA EO only) H_2SO_4 and 0.1 M $HClO_4$ of milli-Q water (18.2 MΩ). While all electrode potentials were physically measured with respect to the Ag/AgCl (3 M) reference electrode, they were all expressed with respect to the reversible hydrogen electrode (RHE) in the figures and text. The conversion numbers are 0.26 V/0.32 V for the 0.5 M/0.1 M H_2SO_4 electrolytes and 0.29 V for the 0.1 M $HClO_4$ electrolyte. These numbers were determined by measuring the open circuit potential between the Ag/AgCl (3 M) reference electrode and the Pt wire electrode under H_2 bubbling. In H_2SO_4, all CO stripping measurements were carried out in a 0.5 M H_2SO_4 supporting electrolyte and all MeOH EO experiments in 0.5 M H_2SO_4 + 0.5 M CH_3OH solution while all FA EO experiments were performed in 0.1 M H_2SO_4 + 0.1 M HCOOH solution. In $HClO_4$, all EC measurements were carried out in a 0.1 M $HClO_4$ supporting electrolyte for CO stripping, in 0.1 M $HClO_4$ + 0.5 M CH_3OH solution for MeOH EO, and in 0.1 M $HClO_4$ + 0.1 M HCOOH solution for FA EO. For CO stripping experiments, the CO was adsorbed by saturating the EC cell with CO for 10 min while holding the electrode potential at 0.1 V *vs.* Ag/AgCl. The cell was then purged with Ar for 30 min before the CO stripping CV was taken. All currents reported were normalized by the Pt surface area calculated by the total hydrogen desorption charge (using 220 μC cm^{-2} for bare Pt black and Pt black/PVP samples). The reproducibility of all measurements within the experimental errors was checked by repeated measurements on at least one more freshly-deposited sample.

In situ IR spectroelectrochemical measurements

In situ FTIR reflection spectroscopic measurements were carried out on a Nexus 870 spectrometer (Nicolet) equipped with an EverGlo IR source and a liquid-nitrogen-cooled MCT-A detector. The Pt NPs samples were drop-cast onto a well-polished, pre-cleaned GC electrode that was pushed against a CaF_2 IR window to form a thin layer solution (~1 μm) and used as the working electrode of a three-electrode IR cell. A saturated calomel electrode (SCE) and a platinized Pt plate were used as the respective reference and counter electrodes. Details of this three-electrode thin-layer IR cell has been described elsewhere.[13] The potential control was achieved by using an EG&G 263A potentiostat/galvanostat. The spectral resolution was set to 8 cm^{-1} and the obtained spectra were shown in the absorbance units defined as $-\log (R_s - R_0)/R_0$ where R_s and R_0 are the spectra taken at the measuring and the reference potentials, respectively. 2000 scans were co-added for each recorded spectrum to improve the signal over noise ratio.

3. Results and discussion

EC characterization

Fig. 1 displays the cyclic voltammograms (CVs) of the 3 catalyst samples (bare Pt black, Pt–PVP12, and Pt–PVP24) in 0.5 M H_2SO_4 (a and b) and in 0.1 M $HClO_4$ (c and d) respectively. The inset in Fig. 1a is the TEM picture of the Pt black that shows that the average size of the NPs was about 3 to 4 nm in

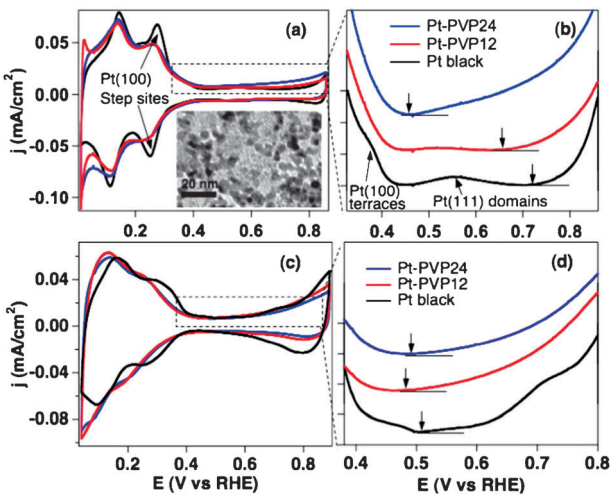

Fig. 1 CVs of the Pt black (black), Pt–PVP12 (red), Pt–PVP24 (blue) samples in 0.5 M H_2SO_4 (a) and 0.1 M $HClO_4$ (c). The highest potential reached in the anodic region was limited to 0.86 V to minimize the electrochemical (EC) decomposition of PVP as well as surface restructuring. The inset in (a) is a TEM image of the Pt black NPs whose size was between 3 to 4 nm. (b)/(d) The expanded view of the area indicated by the rectangle in (a)/(c) with a current scale of 0.005 mA cm^{-2} per division. For clarity, the curves are vertically shifted and the vertical arrows indicate the onsets of the leveling-off current for each sample.

diameter. To prevent surface restructuring, the electrodes were not cycled beyond *ca.* 0.9 V *vs.* RHE and the CVs were recorded before any CO stripping and EO of MeOH and FA experiments were conducted. As it is well-observed, the CV of the commercial Pt black in 0.5 M H_2SO_4 is more structured. It is characterized by 4 distinct features: symmetrical peaks at 0.14 V and 0.29 V, which correspond to (110)- and (100)-type step sites, respectively, a shoulder around 0.39 V, typical of (100) terrace sites and another hump at 0.56 V, characteristic of small (111)-ordered surface domains (Fig. 1b).[14] As PVP was added to the surface, the CV went through significant changes: the peak corresponding to (100) step sites became mostly suppressed (Fig. 1a) and the humps typical of (100) terraces and (111)-ordered surface domains disappeared (Fig. 1b). A similar transformation of the CV was also observed in 0.1 M $HClO_4$ (Fig. 1c and d). These observations are typical of the Pt NP electrocatalysts stabilized by organic ligands[8,10] and are indicative of the preferential adsorption of PVP on certain Pt crystal facets and/or sites[15] and of the changes in the hydrogen adsorption electrochemistry due to electronic effects of the PVP.[16]

Interestingly, the onset of the oxidative current in positive potential scan varied significantly in 0.5 M H_2SO_4: from 0.73 V for Pt black to 0.66 V and 0.48 V for Pt–PVP12 and Pt–PVP24, respectively, as indicated by the vertical arrows in Fig. 1b. The oxidative current in positive potential scan also increased, implying a more oxo-philic surface as compared to the starting pure Pt black in 0.5 M H_2SO_4. The gradual disappearance of the bi-sulfate adsorption induced Pt(111) hump at 0.56 V as the PVP content increased (red to blue curves) indicates that the presence of the latter made the Pt surface much less prone to strong anion adsorption thus more oxo-philic. On the other hand, the shifts of the onset of the oxidative current in 0.1 M $HClO_4$ were much smaller (Fig. 1d): from 0.51 V for Pt black to 0.48 V for Pt–PVP12 to 0.49 V for Pt–PVP24. The PVP also appeared to suppress the amplitude of the oxidative current as the electrode potential increased, more so for higher PVP content. Thus, it made the Pt–PVP samples less oxo-philic as compared to the starting pure Pt black in 0.1 M $HClO_4$. Since the EOs of MeOH, FA, and poisonous CO may rely on the availability of oxygenated species on the surface, these different surface oxidative behaviors are expected to reflect upon the corresponding catalytic activities as we will present below.

The CVs and chronoamperometric (CA) curves of the EO in 0.5 M H_2SO_4 + 0.5 M MeOH are shown in Fig. 2(a) and (b) and those of FA EO in 0.1 M H_2SO_4 in Fig. 2(c) and (d). The most remarkable observation is that there were substantial overall enhancements in the EOs of both MeOH and FA on the Pt–PVP12 and Pt–PVP24 as compared to those of the original Pt black. For the EO of MeOH, the CV peak current of positive potential scan was enhanced 1.5 and 3.6 times while the CA current measured at 60 min showed 3.3 and 6.9 times increases for the Pt–PVP12 and Pt–PVP24, respectively.

The CVs corresponding to the EO of FA are more complicated. There are 3 current peaks at around 0.6 V (Peak I), 0.9 V (Peak II) and 1.4 V (Peak III) in positive potential scan and one broad peak centered at 0.6 V (Peak IV) in negative potential scan, in agreement with previously published

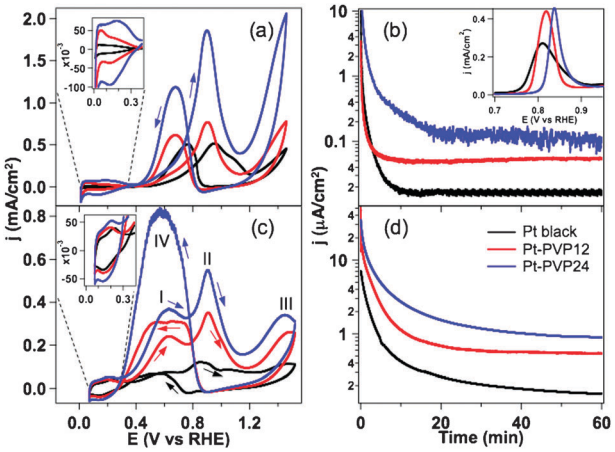

Fig. 2 CVs and CAs of MeOH (a and b) and of FA (c and d) EOs on the Pt black (black), Pt–PVP12 (red), and Pt–PVP24 (blue) NPs in 0.5 M H_2SO_4 + 0.5 M MeOH or 0.1 M H_2SO_4 + 0.1 M FA. The CAs were measured at 0.36 V for the MeOH and at 0.42 V for the FA EOs, respectively. The insets in (a) and (c) show the expanded views of the corresponding hydrogen adsorption/desorption region and the inset in (b) shows the gaseous CO stripping CVs on the three samples.

results.[17,18] Peak I represents the direct EO of FA to CO_2 on the surface sites free of poisonous CO.[19] Peak II corresponds to the EO of surface CO combined with that of FA on the newly freed sites. Peak III accounts for the EO of FA on some catalytically active surface oxides. The Peak IV is usually considered to reflect the real catalytic activity of the surface since both CO and oxides are absent.[17,18] Although all peaks were enhanced on the Pt–PVP samples, Peak IV saw the largest increase compared to that of the Pt black: 4.6 and 12.5 times for Pt–PVP12 and Pt–PVP24, respectively, indicating a significant enhancement in the catalytic activity for the EO of FA. The CA currents measured at 60 min also showed 3.5 and 5.7 times increases respectively.

The CVs and CAs of the EO in 0.1 M $HClO_4$ + 0.5 M MeOH are shown in Fig. 3(a) and (b) and those of FA in Fig. 3(c) and (d). Similar substantial enhancements in the EOs of both MeOH and FA were observed. For the EO of MeOH, the CV peak current in positive potential scan was enhanced 1.8 and 3.6 times while the CA current measured at 60 min showed 2.8 and 6.2 times increases for the Pt–PVP12 and Pt–PVP24, respectively. For the EO of FA, although similar four CV peaks were also observed (Fig. 3c), the degree of enhancement was much higher in 0.1 M $HClO_4$ than in 0.5 M H_2SO_4. Again, the Peak IV showed the largest increase compared to that of the Pt black: 7.7 and 31 times for Pt–PVP12 and Pt–PVP24 respectively. The corresponding enhancements in CA currents measured at 60 min were 4.5 and 8.7 times respectively (Fig. 3d). However, notice that the CV current of Peak I is higher on Pt–PVP12 than on Pt–PVP24, which is in a different order as compared to that in 0.1 M H_2SO_4 (Fig. 2(c)).

It has been well-established that both the EOs of MeOH and FA can have dual, *i.e.*, indirect and direct, reaction pathways among which the indirect one leads to the generation of poisonous CO.[20] Recently, an additional so-called formate reaction pathway was identified for the EO of FA. The adsorbed formate generated in this pathway was considered a bystander

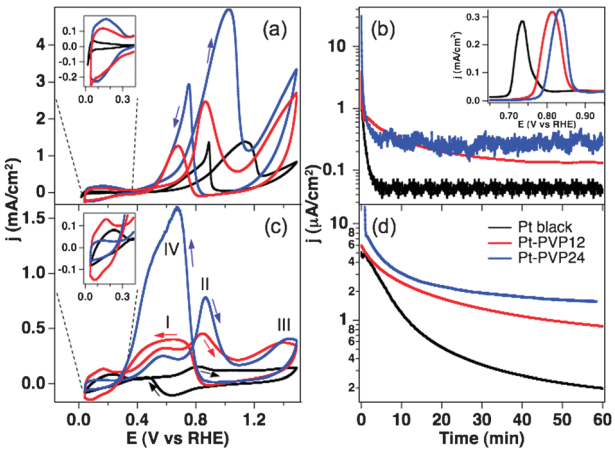

Fig. 3 CVs and CAs of MeOH (a and b) and of FA (c and d) EOs on the Pt black (black), Pt–P VP12 (red) and Pt–PVP24 (blue) NPs in 0.1 M $HClO_4$ + 0.5 M MeOH or 0.1 M FA. The CAs were measured at 0.39 V for the MeOH and at 0.45 V for the FA EOs, respectively. The insets in (a) and (c) show the expanded views of the corresponding hydrogen adsorption/desorption region and the inset in (b) shows the gaseous CO stripping CVs on the three samples.

that most likely was in equilibrium with formate anions/formic acid in solution and could also be further oxidized to CO_2.[18,21] However, the dominant reaction pathways for the EOs of MeOH and FA in the potential range of this study are expected to be very different.[20] The former should follow the indirect reaction pathway with CO as the reaction intermediate ($CH_3OH \rightarrow CO + 3H^+ + 3e^-$) that requires an ensemble of at least 4 Pt atoms while the latter follows a direct reaction pathway ($HCOOH \rightarrow CO_2 + 2H^+ + 2e^-$) that requires only 1 or 2 adjacent Pt atoms and no oxygenated species to be involved. Thus, the observations of the large activity enhancement in two different supporting electrolytes (strong *vs.* weak anion adsorption) for the EOs of *both* MeOH and FA on the Pt–PVP samples as well as of the tunability of this enhancement by varying the amount of adsorbed PVP are highly remarkable and intriguing. This should be contrasted to the fact that alloying Ru to Pt enhances significantly the EO of MeOH but does little to the EO of FA. Thus, we strongly believe that what have been observed here is more than just a simple third-body effect.[22,23]

It is generally accepted that the EO of adsorbed CO follows the Langmuir–Hinshelwood mechanism in which the formation of a surface bound oxygen-containing species, as often represented as Pt–OH, is a prerequisite.[24] In order to electro-oxidize a saturated CO monolayer, the initial generation of such Pt–OH species usually takes place at defect sites, such as step and kink sites. The observed positive shift of the stripping peak of the saturated CO monolayers on the Pt–PVP samples (insets in Fig. 2b and 3b) indicates that the adsorbed PVP interacted primarily with these defect sites and suppressed significantly their Pt–OH generating ability. This is in agreement with the observed changes in CVs induced by the adsorption of PVP (Fig. 1a and c) that indicate that the PVP blocked the Pt(100) step sites.

It is also well known that the EOs of MeOH[9] and FA[17] are more active in $HClO_4$ than in H_2SO_4 because of the lack of strong anion adsorption in the former supporting electrolyte. Since it is highly unlikely that the adsorption of PVP would change significantly the surface morphology of the Pt NPs, the gradual disappearance of the Pt(111) hump at 0.56 V (Fig. 1(b)) is an indication of the PVP-induced blockage of bi-sulfate anion adsorption. This is consistent with the observation that the CO stripping peak potentials changed from 0.73 V in 0.1 M $HClO_4$ and 0.81 V in 0.5 M H_2SO_4 for pure Pt black to 0.81 V and 0.82 V for Pt–PVP12 and 0.83 V and 0.84 V for Pt–PVP24 respectively (insets in Fig. 2b and 3b). That is, the presence of PVP largely eliminated the anion-induced difference and blocked the defect sites for earlier OH adsorption. However, we think that this was not the main cause for the observed catalytic activity enhancements, for two reasons: the first is that the observed enhancement is much larger than the anion-induced difference. The second is that even larger enhancement was observed in 0.1 M $HClO_4$ (Fig. 3).

Although the exact mechanisms responsible for the observed large catalytic activity enhancements are still not fully understood, we believe that it is likely to be the results of two effects that act synergistically in opening more than one reaction pathways (*vide infra*). The first is the enhanced water activation that was brought to bear by the PVP whose hydrophilicity may be further altered by interaction with anions[25,26] in the supporting electrolytes (for instance suppressing strong anion adsorption). As indicated by the vertical arrows in Fig. 1b, the onset potential of the oxidative current negatively shifted from 0.73 V for Pt black to 0.66 V and 0.48 V for Pt–PVP12 and Pt–PVP24 respectively. Similar but much smaller negative shifts were also observed in 0.1 M $HClO_4$: from 0.51 V for Pt black to 0.48 V and 0.49 V for Pt–PVP12 and Pt–PVP24, respectively, as indicated by the arrows in Fig. 1d. These negative shifts are expected to facilitate the elimination of the poisonous CO when the surface is *not* fully covered by CO and enhance the CO tolerance during the EO of MeOH and FA.

The second is the subtle electronic alterations caused by the adsorption of PVP on the surface of Pt NPs, as observed in the previous ^{195}Pt NMR study of the PVP-protected 2.1 nm Pt NPs.[27] The detailed nucleus spin–lattice relaxation measurements of the Pt surface sites clearly showed measurable electronic alterations as compared to those of bare clean Pt surface sites. The slower relaxation rates indicated lower surface Fermi level densities of states that would lead to weakened surface bonding.[28] Recent theoretical calculations also have shown that the support's acid/base properties can have a strong effect on the Pt 5d and 6s, p states and therefore are expected to influence the bonding of the adsorbates.[16] Since it is known that PVP interacts with the Pt surface mainly through its electron rich carbonyl group,[29] observable effects due to electronic alterations on the Pt surface are thus expected. Similar organic-ligand triggered electronic alterations were also reported recently.[8]

Indeed, as can be clearly seen in the insets of Fig. 2a and 3a where the expanded views of hydrogen adsorption/desorption are shown, the surfaces of the Pt–PVP12 and Pt–PVP24 were much less poisoned by CO during the EO of MeOH: the percentages of the blocked sites are 83%, 35%, and 13% in sulfuric acid and 68%, 18%, and 10% in perchloric acid for Pt

black, Pt–PVP12, and Pt–PVP24 respectively. In other words, the two Pt–PVP samples were much more CO-tolerant, thus led to the much enhanced EO activity of MeOH in both electrolytes as measured by the CV peak currents and the long-term CA currents (Fig. 2a and b and 3a and b). On the other hand, while the enhanced CO tolerance, as discussed above, may also be used to rationalize the enhanced long-term steady-state EO currents of FA (Fig. 2d and 3d) where the CO poisoning is the main concern, interpreting the site blocking of hydrogen adsorption as revealed by the corresponding insets in Fig. 2c and 3c isn't as straightforward. As shown in the insets, the amounts of the blocked sites were 98%, 93%, and 93% in 0.5 M H_2SO_4 (Fig. 2c), and 46%, 80%, 92% in 0.1 M $HClO_4$ (Fig. 3c) for Pt black, Pt–PVP12, and Pt–PVP24 respectively. Notably, the site-blocking trend was actually reversed in 0.1 M $HClO_4$: the Pt–PVP24 had the least amount of unblocked sites, despite its largest Peak IV current. This reverse of trend might be indicative of an electrolyte-dependent adsorption of formate,[18,20] *i.e.*, the difference in anion (ClO_4^-)-PVP interaction[25,26] may cause increased formate adsorption in 0.1 M $HClO_4$ as the amount of adsorbed PVP increased.

In situ IR spectroelectrochemical characterization

In order to shed more mechanistic insights into the above described and somewhat unexpected catalytic enhancements, we carried out a rather detailed *in situ* IR investigation of the systems in 0.1 M H_2SO_4, focusing on the adsorbed CO and reaction-produced CO_2. Fig. 4 shows the IR spectra taken at 0.312 V (*vs.* RHE) of the CO adsorbed on Pt-black, Pt–PVP12, and Pt–PVP24 from gaseous CO (a), generated from MeOH dissociation (b) and from FA dissociation (c). Although somewhat noisy, the CO stretching peak position can still be unambiguously identified and the wavenumbers are 2072 cm^{-1}, 2073 cm^{-1}, 2064 cm^{-1} for gaseous CO, 2059 cm^{-1}, 2046 cm^{-1}, and 2041 cm^{-1} for MeOH CO, and 2063 cm^{-1}, 2062 cm^{-1}, and 2072 cm^{-1} for FA CO on Pt black, Pt–PVP12, abd Pt–PVP24 respectively. No clear pattern was observed, though the frequencies are of typical values for linearly bound CO (*i.e.*, atop CO).[30–33] The variations in the frequency may reflect the differences in the local as well as overall CO coverage (*vide infra*).

The changes in the (normalized) amount of the adsorbed CO and the EO-produced CO_2 as a function of the electrode potential as measured by their respective IR intensity are presented in Fig. 5(a)–(c). For the adsorbed gaseous CO, Fig. 5(a), the amount of the adsorbed CO didn't change substantially until the start of the EO. The subsequent decrease in the surface-bound CO synchronized with the increase in the reaction-produced CO_2. This indicates that the adsorbed CO was oxidized directly to CO_2. Also, the EO of the adsorbed CO on the Pt black took place at the lowest electrode potential, which was followed by that on the Pt–PVP24 and Pt–PVP12 respectively. This order is different from that shown in the inset of Fig. 2b (Pt black, Pt–PVP12, and Pt–PVP24), which is probably due to the different concentrations of H_2SO_4 used: 0.1 M for the former (to avoid erosion of the CaF_2 optical window) but 0.5 M for the latter. It is well-know that higher concentration of H_2SO_4 generates stronger bisulfate adsorption[34,35] which is manifested in the much higher EO potential in the latter case ($\sim$0.82 V *vs.* $\sim$0.6 V). But one thing in common in both cases is that the effect of PVP is clearly evidenced: the presence of adsorbed PVP delayed generally the EO of adsorbed CO, probably by blocking the defect sites (*vide supra*) that delayed the generation of Pt–OH species needed for CO oxidation.

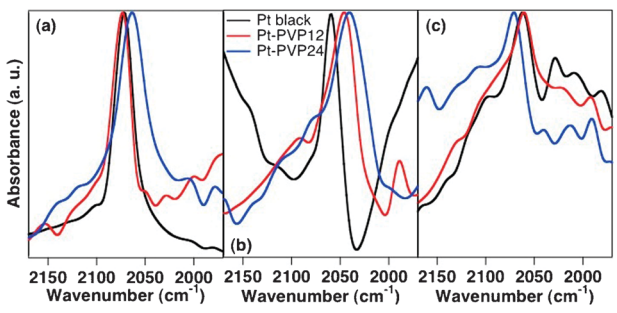

Fig. 4 *In situ* IR spectra of the adsorbed CO of gaseous CO (a), MeOH CO (b), and FA CO (c) taken at 0.312 V (*vs.* RHE) in 0.1 M H_2SO_4 for the Pt black (black), Pt–PVP12 (red), and Pt–PVP24 (blue).

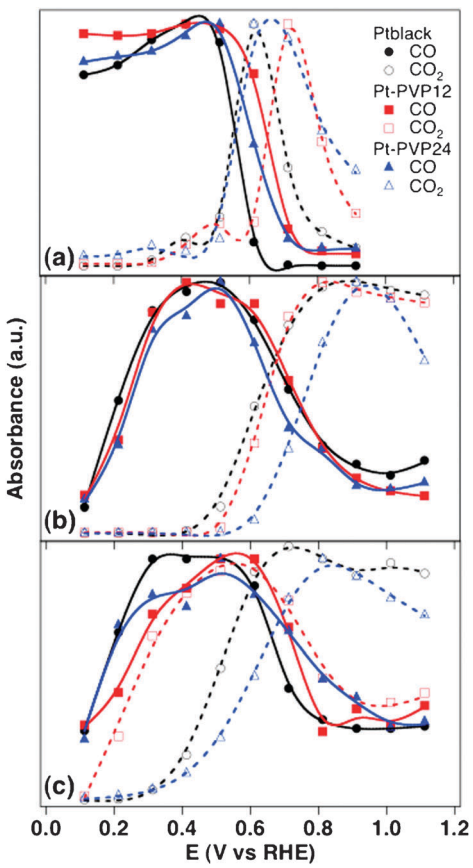

Fig. 5 Changes in the (normalized) amount of CO adsorbed (solid curves) on Pt surface and CO_2 produced (dashed curves) as a function of electrode potential for gaseous CO (a), MeOH CO (b), and FA CO (c) for Pt black (black solid and open circles), Pt–PVP12 (red solid and open squares), and Pt–PVP24 (blue solid and open triangles) respectively. The solid and dashed curves are only for eye-guiding purpose.

For the EO of MeOH, Fig. 5(b), the amount of the adsorbed CO accumulated first as the electrode potential increased, reached maximum at ~0.5 V, then decreased monotonically farther as the potential increased. The most intriguing observation is that while the decrease in the adsorbed CO on the Pt black and Pt–PVP12 synchronized with the increase in the produced CO_2 as was for the adsorbed gaseous CO (Fig. 5(a)), there was a clear delay in the CO_2 production on the Pt–PVP24: the early drop in the adsorbed CO was not accompanied by the increase in the CO_2 production. This delay implies strongly that a different reaction pathway was operational in the Pt–PVP24 case, probably $CO_{ad} \rightarrow (HCHO)_{ad}$ or/and $(HCOO)_{ad} \rightarrow CO_2$.[20] This may explain the lower amount of the adsorbed CO and higher activity observed in Fig. 2(a) and (b).

For the EO of FA, Fig. 5(c), evidence of different operational reaction pathway(s) is also ostensible. As expected, the amount of the adsorbed CO accumulated as the dissociation of FA took place at lower electrode potentials (< ~0.5 V). However, the production of CO_2 was very different for the three samples. For the Pt–PVP12 (red), the production of CO_2 took off at an electrode potential as low as 0.2 V and it followed closely the changing trend of the adsorbed CO, indicating a direct oxidation of CO to CO_2, *i.e.*, a dominant indirect (*via* CO_{ad}) reaction pathway.[18,33] Consequently, the accumulation of the adsorbed CO did not show a plateau as did the other two samples. For the Pt black (black), although the production of CO_2 was delayed as compared to that on the Pt–PVP12, it took off at an electrode potential (~0.4 V) that was much more negative than the potential at which (~0.5 V) the plateau of the adsorbed CO started dropping down. That is, the production of CO_2 below 0.5 V did not happen *via* the adsorbed CO, *i.e.*, a direct reaction pathway was operational (such as $HCOOH \rightarrow HCOO \rightarrow CO_2$).[18,21] For the Pt–PVP24, the production of CO_2 was slightly further delayed but otherwise behaved in a similar fashion as the Pt black. And, the formate (HCOO) pathway could lead to more adsorbed formate that blocked more sites for hydrogen adsorption.

The presence of PVP also manifested its effect on the Stark tuning of the C–O stretching frequency which is shown in Fig. 6. For CO adsorbed on Pt in an electrochemical environment, its stretching frequency is a function of both CO coverage[36] and potential[37]: it increases as the electrode potential or CO coverage increases. Once the oxidation of the adsorbed CO starts, these two effects go oppositely and cancel each other as the electrode potential moves further positively. Therefore in Fig. 6, only the points before the CO oxidation started are used to calculate the Stark tuning rates.

For the adsorbed gaseous CO, the C–O stretching frequencies were generally high, resulted from a high total CO coverage as expected for gaseous adsorption. Individually, the frequency followed the order Pt–PVP12 > Pt black > Pt–PVP24. The corresponding Stark tuning rates were 10 cm^{-1} V^{-1}, 29 cm^{-1} V^{-1}, and 16 cm^{-1} V^{-1}, respectively. Notice that the value for the Pt black is consistent with values reported in the literature.[5,10,11] We speculate that the adsorbed CO would tend to form locally more compact structure in the presence of PVP thus lead to higher C–O frequency and lower Stark tuning rate. On the other hand, as the amount of PVP increased, the overall CO coverage would still decrease, thus lead to lower C–O stretching frequency and higher Stark tuning rate in Pt–PVP24 as compared to Pt–PVP12.

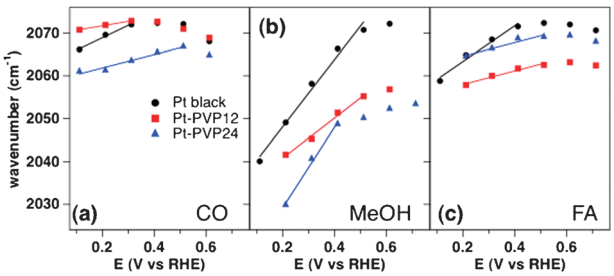

Fig. 6 The corresponding (to Fig. 5) Stark tuning effects are shown in (a)–(c) with the following slopes for the straight lines shown: 29 cm^{-1} V^{-1}, 10 cm^{-1} V^{-1}, and 16 cm^{-1} V^{-1} for the gaseous CO (a); 79 cm^{-1} V^{-1}, 47 cm^{-1} V^{-1}, and 94 cm^{-1} V^{-1} for the MeOH CO (b); and 42 cm^{-1} V^{-1}, 16 cm^{-1} V^{-1}, and 16 cm^{-1} V^{-1} for the FA CO (c) for Pt black (black circles), Pt–PVP12 (red squares), and Pt–PVP24 (blue triangles), respectively.

For the adsorbed MeOH CO, the coverage is usually low and according to the expanded view in Fig. 2(a) for the samples studied here, the CO coverage decreased in the following order, Pt black > Pt–PVP12 > Pt–PVP24. This would explain the frequency order observed in Fig. 6(b). The much higher Stark tuning rates may be rationalized by the increase of CO coverage before 0.5 V (see Fig. 5(b)) and the true electrode-potential-caused Stark tuning effect. The same reasoning can also be applied to the adsorbed FA CO (Fig. 6(c)). According to the C–O frequencies, the overall CO coverage of the adsorbed FA CO would be much higher than the adsorbed MeOH CO but slightly lower than the adsorbed gaseous CO. Individually, one would expect to have the following order of the CO coverage, again according to the frequency differences: Pt black > Pt–PVP24 > Pt–PVP12. This order is in agreement with the observation that the CO oxidation on the Pt–PVP12 happened much earlier as shown in Fig. 5(c).

The effect of PVP on the reactivity of MeOH and FA EOs was further investigated by following the time-resolved reaction kinetics with *in situ* IR of the reaction-produced CO_2 (Fig. 7) for the EO of FA: (a) with a potential step from 0.062 V to 0.312 V and (b) with a potential step from 0.062 V to 0.612 V, and for the EO of MeOH (c) with a potential step from

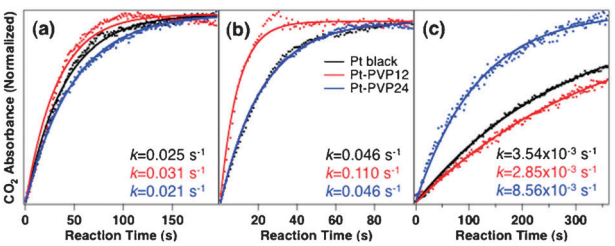

Fig. 7 EO reaction kinetics for (a) FA EO with a potential step from 0.062 V to 0.312 V (*vs.* RHE), (b) FA EO with a potential step from 0.062 V to 0.612 V, and (c) MeOH EO with a potential step from 0.062 V to 0.612 V. The solid curves are the fits to a first order reaction kinetic model $P = P_0(1 - \exp(-kt))$ where k is the reaction rate constant and P_0 is the normalization constant. The reaction rate constants obtained from the fits are shown in the respective figures.

0.062 V to 0.612 V. All the kinetic data can be fitted reasonably well by a first order reaction kinetic model $P = P_0[1 - \exp(-kt)]$ where k is the reaction rate constant (solid curves in Fig. 7 in which all curves were normalized by P_0). As can be seen in Fig. 7(a) and (b), the activity for generating CO_2 was highest on the Pt–PVP12, lowest on the Pt–PVP24, with the Pt black in the middle which is in full agreement with the data shown in Fig. 5(c). However, it disagrees with the data shown in Fig. 2(c) and (d) where the Pt–PVP24 showed the highest activity. This discrepancy may be reconciled by realizing that the data in Fig. 2(c) and (d) measured the total activity from all possible reaction pathways but the data in Fig. 7(a) and (b) measured only those that produced CO_2. An alternative or additional reason could be the different concentrations of H_2SO_4 used. Notice that in 0.1 $HClO_4$, the FA EO activity was actually higher on the Pt–PVP12 than on the Pt–PVP24 in positive potential scan up to 0.8 V (Fig. 3(c)).

On the other hand, the data in Fig. 7(c) show that the Pt–PVP24 had the highest activity for the MeOH EO, more than twice higher than both the Pt–PVP12 and the Pt-black, which is in agreement with the data shown in Fig. 2(a) and (b). Notice that the FA EO reached the steady-state much faster than the MeOH EO on these Pt NPs, indicating a much faster reaction kinetics.

4. Conclusions

In conclusion, we reported here some unexpected yet highly intriguing observations of the capping polymer (PVP)-enhanced electrocatalytic activity of the Pt NPs for the EOs of both MeOH and FA and in two different supporting electrolytes. It is remarkable that both the transient intrinsic EO activities as measured by the CVs (Fig. 2b and 3b) and the CO-poisoning tolerant steady-state currents as measured by CAs (Fig. 2d and 3d) in both electrolytes were substantially enhanced.

We also reported *in situ* IR investigation of the PVP effect focusing on the adsorbed CO and reaction-produced CO_2 which has provided deeper mechanistic insights into the effect of the adsorbed PVP. It suggests strongly that the observed activity enhancements are highly likely due to the PVP-induced additional reaction pathways for both the MeOH and FA EOs, probably MeOH $\rightarrow$ CO_{ad} $\rightarrow$ $(HCHO)_{ad}$ or/and $(HCOO)_{ad}$ $\rightarrow$ CO_2 (lead to much less adsorbed CO) for the former and HCOOH $\rightarrow$ HCOO $\rightarrow$ CO_2 for the latter.

Although the presence of the PVP rendered some Pt NPs electrochemically inactive as indicated by the decrease in the absolute hydrogen desorption charges, the enhanced activity was so high that the Pt–PVP samples still demonstrated much (2 to 3 times) higher mass specific activities (see Tables S1–S3 in the ESI† for details) that are more relevant for practical applications. It is well known that strongly bound species, such as CO and sulfur, generally poison the catalytic surfaces. Suitable weaker interactions that would enable a tuning of the catalytic activity at a *finer* scale are highly desirable but currently lacking. The results reported in this article provide a compelling case that demonstrates that PVP and similar ligands may fill up this vacuum. In this regard, how the interaction between PVP and anions of supporting electrolytes can be used as an additional dimension of activity tunability should be a topic of high interest. Most importantly, such an operando may open up a new paradigm of research in which the protecting/stabilizing organic ligands can now be incorporated as an advantageous part of a nanocatalytic system.

Acknowledgements

DJC is partially supported by a CSC (Chinese Scholar Council, 2009631048) graduate fellowship. The research in the Sun lab is supported by NSFC (20921120405, 21021002), and the research in the Tong lab is supported by DOE (DE-FG02-07ER15895) and by NSF (CHE-0923910). YYJT is also a recipient of a Chinese Oversea Collaborative Research grant from the NSFC (20828005). The authors also thank gratefully Dr Paul Maupin from DOE-BES for stimulating discussions on anions-polymer interaction.

Notes and references

1 R. Narayanan and M. A. El-Sayed, *J. Am. Chem. Soc.*, 2003, **125**, 8340.
2 R. Narayanan and M. A. El-Sayed, *J. Phys. Chem. B*, 2005, **109**, 12663.
3 *Applied Homogeneous Catalysis with Organometallic Compounds*, ed. B. Cornils and W. A. Herrman, Wiley-VCH, Weinheim, 1996.
4 Y. Gu, J. St-Pierre and H. J. Ploehn, *Langmuir*, 2008, **24**, 12680.
5 H. Lang, R. A. May, B. L. Iversen and B. D. Chandler, *J. Am. Chem. Soc.*, 2003, **125**, 14832.
6 I. Lee, R. Morales, M. A. Albiter and F. Zaera, *Proc. Natl. Acad. Sci. U. S. A.*, 2008, **105**, 15241.
7 C. N. Kostelansky, J. J. Pietron, M.-S. Chen, W. J. Dressick, K. E. Swider-Lyons, D. E. Ramaker, R. M. Stroud, C. A. Klug, B. S. Zelakiewicz and T. L. Schull, *J. Phys. Chem. B*, 2006, **110**, 21487.
8 J. J. Pietron, Y. Garsany, O. Baturina, K. E. Swider-Lyons, R. M. Stroud, D. E. Ramaker and T. L. Schull, *Electrochem. Solid-State Lett.*, 2008, **11**, B161.
9 C. Susut, G. B. Chapman, G. Samjeske, M. Osawa and Y.-Y. Tong, *Phys. Chem. Chem. Phys.*, 2008, **10**, 3712.
10 Z. Q. Tian, S. P. Jiang, Z. Liu and L. Li, *Electrochem. Commun.*, 2007, **9**, 1613–1618.
11 H. Song, F. Kim, S. Connor, G. A. Somorjai and P. Yang, *J. Phys. Chem. B*, 2005, **109**, 188.
12 H. A. Gasteiger, S. S. Kocha, B. Sompalli and F. T. Wagner, *Appl. Catal., B*, 2005, **56**, 9.
13 S. G. Sun and Y. Lin, *Electrochim. Acta*, 1998, **44**, 1153–1162.
14 J. Solla-Gullon, F. J. Vidal-Iglesias, E. Herrero, J. M. Feliu and A. Aldaz, *Electrochem. Commun.*, 2006, **8**, 189.
15 N. M. Markovic and P. N. Ross, *Surf. Sci. Rep.*, 2002, **45**, 117–229.
16 M. K. Oudenhuijzen, J. A. van Bokhoven, D. E. Ramaker and D. C. Koningsberger, *J. Phys. Chem. B*, 2004, **108**, 20247–20254.
17 G. Q. Lu, A. Crown and A. Wieckowski, *J. Phys. Chem. B*, 1999, **103**, 9700.
18 Y. X. Chen, M. Heinen, Z. Jusys and R. J. Behm, *Langmuir*, 2006, **22**, 10399–10408.
19 A. Capon and R. Parsons, *J. Electroanal. Chem.*, 1973, **44**, 239.
20 M. Neurock, M. Janik and A. Wieckowski, *Faraday Discuss.*, 2009, **140**, 363.
21 Y. X. Chen, M. Heinen, Z. Jusys and R. J. Behm, *Angew. Chem., Int. Ed.*, 2006, **45**, 981–985.
22 F. Huerta, E. MorallÛn, C. Quijada, J. L. V·zquez and A. Aldaz, *Electrochim. Acta*, 1998, **44**, 943–948.
23 A. Cuesta, *J. Am. Chem. Soc.*, 2006, **128**, 13332–13333.
24 B. E. Hayden, D. Pletcher, J.-P. Suchsland and L. J. Williams, *Phys. Chem. Chem. Phys.*, 2009, **11**, 1564–1570.
25 J. D. Song, R. Ryoo and M. S. Jhon, *Macromolecules*, 1991, **24**, 1727–1730.
26 A. Güner, *J. Appl. Polym. Sci.*, 2000, **75**, 1434–1439.
27 Y.-Y. Tong, T. Yonezawa, N. Toshima and J. J. v. d. Klink, *J. Phys. Chem.*, 1996, **100**, 730.

28 Y.-Y. Tong, H. S. Kim, P. K. Babu, P. Waszczuk, A. Wieckowski and E. Oldfield, *J. Am. Chem. Soc.*, 2002, **124**, 468–473.
29 Y. Borodko, S. M. Humphrey, T. D. Tilley, H. Frei and G. A. Somorjai, *J. Phys. Chem. C*, 2007, **111**, 6288.
30 Q. S. Chen, A. Berna, V. Climent, S. G. Sun and J. M. Feliu, *Phys. Chem. Chem. Phys.*, 2010, **12**, 11407–11416.
31 T. Yajima, H. Uchida and M. Watanabe, *J. Phys. Chem. B*, 2004, **108**, 2654–2659.
32 M. Arenz, V. Stamenkovic, P. N. Ross and N. M. Markovic, *Surf. Sci.*, 2004, **573**, 57–66.
33 M. Arenz, K. J. J. Mayrhofer, V. Stamenkovic, B. B. Blizanac, T. Tomoyuki, P. N. Ross and N. M. Markovic, *J. Am. Chem. Soc.*, 2005, **127**, 6819–6829.
34 A. Lachenwitzer, N. Li and J. Lipkowski, *J. Electroanal. Chem.*, 2002, **532**, 85–98.
35 D.-M. Zeng, Y.-X. Jiang, Z.-Y. Zhou, Z.-F. Su and S.-G. Sun, *Electrochim. Acta*, 2010, **55**, 2065–2072.
36 S. Chang, L. Leung and M. Weaver, *J. Phys. Chem.*, 1989, **93**, 5341–5345.
37 D. Lambert, *Electrochim. Acta*, 1996, **41**, 623–630.

